

# Numerical Modeling and Optimization of Electric Field Distribution in Subcutaneous Tumor Treated With Electrochemotherapy Using Needle Electrodes

Selma Corovic, Anze Zupanic, and Damijan Miklavcic

**Abstract**—Electrochemotherapy (ECT) is an effective antitumor treatment employing locally applied high-voltage electric pulses in combination with chemotherapeutic drugs. For successful ECT, the entire tumor volume needs to be subjected to a sufficiently high local electric field, whereas, in order to prevent damage, the electric field within the healthy tissue has to be as low as possible. To determine the optimum electrical parameters and electrode configuration for the ECT of a subcutaneous tumor, we combined a 3-D finite element numerical tumor model with a genetic optimization algorithm. We calculated and compared the local electric field distributions obtained with different geometrical and electrical parameters and different needle electrode geometries that have been used in research and clinics in past years. Based on this, we established which model parameters had to be taken into account for the optimization of the local electric field distribution and included them in the optimization algorithm. Our results showed that parallel array electrodes are the most suitable for the spherical tumor geometry, because the whole tumor volume is subjected to sufficiently high electric field while requiring the least electric current and causing the least tissue damage. Our algorithm could be a useful tool in the treatment planning of clinical ECT as well as in other electric field mediated therapies, such as gene electrotransfer, transdermal drug delivery, and irreversible tissues ablation.

**Index Terms**—Electrochemotherapy (ECT), electropermeabilization, finite element method, genetic algorithm, optimization, subcutaneous tumor.

## I. INTRODUCTION

**E**LECTROCHEMOTHERAPY (ECT) is a nonthermal and local tumor treatment, clinically proven to be effective, safe, and well tolerated by patients [1], [2]. ECT standard operating procedures have been defined for the treatment of cutaneous and subcutaneous tumor nodules of different histologies. Numerous published research and clinical reports have shown that it can be used as an efficient local tumor treatment for various tumor types [3]–[8].

ECT is performed using either intravenous or intratumoral chemotherapeutic injection, followed by the application of

high-voltage electric pulses locally delivered to the target tissue via appropriate sets of electrodes. Electric pulses induce a local electric field ( $E$ ) within the treated tissue, which depends on the tissue's electrical and geometrical properties. Namely, for efficient ECT, it is necessary that the entire tumor tissue is subjected to a local electric field in the range between reversible and irreversible electropermeabilization threshold values ( $E_{\text{rev}} < E < E_{\text{irrev}}$ ), which causes transient structural changes in cell membranes (termed reversible electropermeabilization) and allows for increased entrance of chemotherapeutics into target tissues. This increased membrane permeabilization potentiates the effect of chemotherapeutic drugs, thus significantly lowering the required dose and improving the effectiveness of the treatment [9]. Other requirements for efficient ECT are that the healthy tissue volume subjected to  $E > E_{\text{rev}}$  has to be kept minimal so as not to expose the healthy tissue to an  $E$  higher than necessary and to prevent the excessive irreversible tissue damage ( $E > E_{\text{irrev}}$ ). At the same time, the electric current through the tissue has to be as low as possible due to the technical limitations of the high voltage pulse generator.

The magnitude and distribution of local electric field and thus the degree of tissue electropermeabilization can be controlled by electrode configuration and polarity and the amplitude of electric pulses [10], [11]. Local electric field, however also depends on the geometrical and electrical properties of treated tissues; therefore, both have to be taken into account when planning the treatment. Electrode types currently most often used for therapeutic and research purposes are external parallel plate electrodes and different geometries of needle electrode arrays [6], [12]–[14]. External plate electrodes are suitable for the treatment of protruding cutaneous tumors as the local electric field can be easily controlled by the contact surface between electrodes and the treated tissue, the interelectrode distance, and the amplitude of the applied electric pulses. If the target tissue cannot be fixed between the electrodes or is seated in deeper tissue, an array of needle electrodes is more effective as it can penetrate into the tissue to assure the necessary magnitude of electric field within the deeper parts of the tumor. The choice of the suitable electrode type and geometry can be determined by means of a numerical model [13], [15]. Numerical modeling can therefore serve as a vital component in ECT treatment planning; moreover, it can predict the treatment outcome for each tumor type with its specific electrical and geometrical properties, as has already been demonstrated [16].

Manuscript received November 14, 2007; revised April 19, 2008. This work was supported in part by the European Commission under FP6 Grant ANGIOSKIN LSHB-CT-2005-512127 and in part by the Slovenian Research Agency.

The authors are with the Faculty of Electrical Engineering, University of Ljubljana, 1000 Ljubljana, Slovenia (e-mail: selma.corovic@fe.uni-lj.si; anze.zupanic@fe.uni-lj.si; damijan.miklavcic@fe.uni-lj.si).

Color versions of one or more of the figures in this paper are available online at <http://ieeexplore.ieee.org>.

Digital Object Identifier 10.1109/TPS.2008.2000996

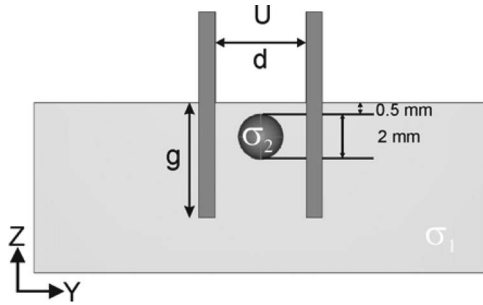


Fig. 1. Central  $YZ$  view across the subcutaneous tumor model, where  $U$  is the applied voltage between the electrode rows,  $g$  is the depth of needle insertion,  $d$  is the distance between the electrodes as shown in Fig. 3, and  $\sigma_1$  and  $\sigma_2$  are the healthy and tumor tissue conductivities, respectively. The tumor is positioned 0.5 mm below the surface of the model.

In this paper, we used finite element method and genetic algorithm to investigate and optimize the local electric field distribution within a given 3-D model of a subcutaneous tumor. The electric properties of the modeled tissues are based on the fact that the tumor tissue is more conductive than its surrounding healthy tissue [16], [17]. We investigated the influence of the number of needle electrodes, depth of electrode insertion, configuration of electrodes with respect to the treated tissue, and amplitude of electric pulses. We quantified local electric field distribution inside the tumor and its surrounding healthy tissue obtained with four needle electrode geometries that have been used in clinics and research in past years [1], [14], [18]. Based on the calculated distributions of electric field, we established which model parameters had to be taken into account for the optimization of the local electric field distribution and included them in the genetic optimization algorithm that we developed in order to determine the optimum electrode configuration in the target tissue. As the output of the algorithm, we obtained the optimum solution of the analyzed treatment parameters. Our algorithm can be used in local electric field optimization and thus in ECT treatment planning for arbitrary tumor geometries and electrical properties. Our optimization approach can be beneficial also in the treatment planning of other electric field mediated treatments, such as gene electro-transfer [19], transdermal drug delivery [20], and tissue ablation treatments [21].

## II. METHODS

### A. Tissue Properties and Model Geometry

Our model of a subcutaneous tumor consisted of two tissues, the target tumor tissue (a sphere with a diameter of 2 mm), and its surrounding healthy tissue (Figs. 1–3). Both tissues were considered isotropic and homogeneous, the assigned conductivity values being 0.4 S/m for the tumor and 0.2 S/m for the healthy tissue. These values describe the conductivity at the end of the electroporation process. The values were chosen in accordance with previous measurements of tumor and tissue conductivity and models of subcutaneous tumor and skin electroporation [16], [17], [19].

The electric field distribution was calculated for four different electrode geometries: three different parallel needle electrode arrays [Fig. 2(a)–(c)] and a hexagonal electrode array

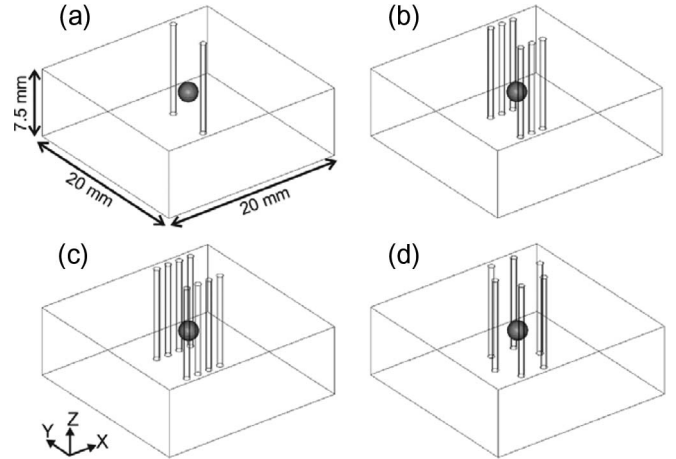


Fig. 2. Three-dimensional geometry of subcutaneous tumor with four needle electrode geometries analyzed: (a) One needle electrode pair, (b) three needle electrode pairs, (c) four needle electrode pairs, and (d) hexagonal needle electrode array.

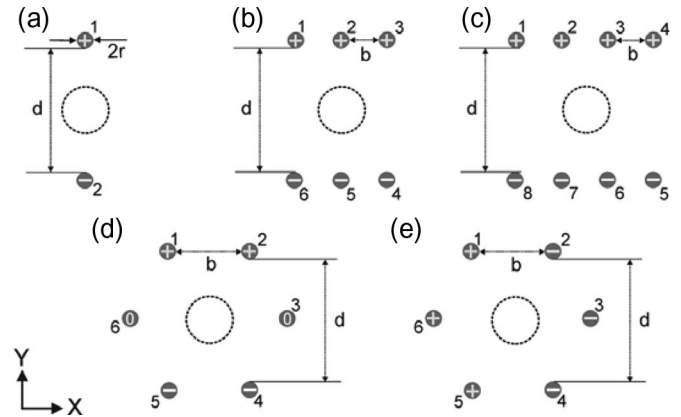


Fig. 3.  $XY$  view of the model with electrode geometries, polarities, and arrangement with respect to (the circled region) the target/tumor tissue: (a) One needle electrode pair, (b) three needle electrode pairs, (c) four needle electrode pairs, (d)  $2 \times 2$  hexagonal needle electrode array (two electrodes on positive potential, two on negative potential, and two grounded), and (e)  $3 \times 3$  hexagonal needle electrode array (three electrodes on positive potential and three on negative potential).  $d$  and  $b$  stand for the distance between opposite sets of electrodes and distance between electrodes of the same row (parallel needle electrode arrays) or distance between neighboring electrodes (hexagonal needle electrode array), respectively.

[Fig. 2(d)], and five electrode polarities: three for the parallel needle electrode arrays [Fig. 3(a)–(c)] and two for the hexagonal electrode array [Fig. 3(d) and (e)]. These geometries and polarities were chosen as they are the most often used in ECT research and therapy.

### B. Numerical Modeling

All numerical calculations were performed with a commercial finite element software package COMSOL Multiphysics 3.3a (COMSOL AB, Sweden) and run on a desktop PC (Windows XP, 3.0-GHz Pentium 4, 1-GB RAM). Electric field distribution in the tissue, caused by an electric pulse, was determined by solving the Laplace equation for static electric currents

$$-\nabla \cdot (\sigma \cdot \nabla \varphi) = 0 \quad (1)$$

where  $\sigma$  and  $\varphi$  stand for the electric conductivity of the tissue and electric potential, respectively. The boundary conditions used in our calculations were a constant potential on the surface of the electrodes (Fig. 3) and electric insulation on all outer boundaries of the model. Results were controlled for numerical errors by increasing the size of our model and increasing the mesh density, until the electric insulation condition and error due to meshing irregularities were insignificant—a further increase in domain size or mesh density only increased the computation time; however, the results changed less than 0.5%.

The electric field distributions obtained in our models were displayed in the range from the reversible  $E_{\text{rev}} = 400$  V/cm to the irreversible electropermeabilization threshold value  $E_{\text{irrev}} = 900$  V/cm. These values were taken from a previously published study, in which we estimated them by comparing *in vivo* measurements and the numerical modeling of the electropermeabilization of a subcutaneous tumor [16], [22]. Namely,  $E_{\text{rev}}$  was estimated to be the same for the tumor and skin tissue (400 V/cm), whereas the  $E_{\text{irrev}}$  values were estimated to be 800 and 1000 V/cm for the tumor and skin, respectively. The  $E_{\text{irrev}}$  in our model was set as the average of these two values (900 V/cm) in the tumor and healthy tissue.

### C. Optimization

The genetic algorithm [23] was written with MATLAB 2007a (Mathworks, USA) and run together with the numerical calculation using the link between MATLAB and COMSOL. The initial population of chromosomes (vectors of real numbers:  $X = (x_1, x_2, \dots, x_n)$ ) was generated randomly, taking into account the following model constraints: range of distances between electrodes, range of depth of electrode insertion into tissue, and range of voltages between the electrodes. These constraints were chosen so that the calculation domain size, COMSOL meshing capabilities, and oncology experts' demands for a safety margin [24], when treating solid tumors, were all respected. Chromosomes for reproduction were selected proportionally to their fitness, according to the fitness function

$$F = 12 + 100 \cdot V_{\text{Trev}} - 10 \cdot V_{\text{Hirrev}} - V_{\text{Hrev}} - V_{\text{Tirrev}} \quad (2)$$

where  $F$  stands for fitness,  $V_{\text{Trev}}$  and  $V_{\text{Tirrev}}$  stand for tumor volume subjected to the local electric field above  $E_{\text{rev}}$  and  $E_{\text{irrev}}$ , respectively, and  $V_{\text{Hrev}}$  and  $V_{\text{Hirrev}}$  stand for the volume of healthy tissue subjected to local electric field above  $E_{\text{rev}}$  and  $E_{\text{irrev}}$ , respectively. The weights in the fitness function were set accordingly to the importance of the individual parameters for efficient ECT. Namely,  $V_{\text{Trev}}$  is crucial for efficient ECT; therefore, its weight is largest (100) in comparison to the weight of  $V_{\text{Hirrev}}$  (10), which was in turn larger than the weights of  $V_{\text{Hrev}}$  and  $V_{\text{Tirrev}}$ , as their significance for successful ECT is still debated. Other weight values that kept a similar ratio gave similar results. The integer 12 is present only to assure that the fitness function is always positive.

The selected chromosomes reproduced by crossover or mutation. When crossover takes place, each new chromosome

TABLE I  
GENETIC ALGORITHM PARAMETERS

Size of initial population	Number of generations	Fraction of elite chromosomes [%]	Probability of cross-over	Probability of mutation
20 - 30	100	10	0.95	0.05

$Z = (z_1, z_2, \dots, z_n)$  is a random linear combination of parent chromosomes  $X$  and  $Y$

$$z_i = a_i \cdot x_i + (1 - a_i) \cdot y_i, \quad a_i \in [0, 1]. \quad (3)$$

When mutation takes place, each new chromosome  $M = (m_1, m_2, \dots, m_n)$  is a random variation of one parent chromosome  $X$

$$m_i = x_i + b_i \cdot x_i, \quad b_i \in [-0.3, 0.3]. \quad (4)$$

Crossover and mutation were chosen according to the probabilities in Table I, with the exception that the top ranking solutions (elite) could not be subjected to mutation. The genetic algorithm was terminated after 100 generations, when the fitness of the highest ranking solution usually reached a plateau. The algorithm always converged to a possible optimum solution. The average computation time of the algorithm was two hours. Other genetic algorithm parameters can be found in Table I.

### D. Protocol

To select the optimum electrode configuration for ECT of the subcutaneous tumor model, we first analyzed the local electric field distribution inside the tissue model for several discrete values of applied voltage between electrodes for all electrode geometries and polarities (Fig. 3). Distance between opposite sets of electrodes  $d$  and distance between electrodes of the same row  $b$  (parallel needle electrode arrays) or distance between neighboring electrodes  $b$  (hexagonal needle electrode array) were kept constant, at  $b = 0.65$  mm (parallel arrays),  $b = 4/\sqrt{3}$  mm (hexagonal array), and  $d = 4$  mm, in all simulations. For each electrode geometry and two electrode depths ( $g = 3$  mm—as deep as the bottom of the tumor;  $g = 5$  mm—double the depth of the tumor), we calculated the minimum voltage  $U_c$  (critical voltage) that had to be applied between the electrodes so that the minimum electric field over the entire tumor volume exceeded  $E_{\text{rev}}$ . This was done by a sequence of calculations, in which we decreased the voltage by increments of 10 V, until the lowest needed amplitude was reached. We then selected the calculated critical voltage  $U_c$  that resulted in the lowest calculated values of reversibly electropermeabilized volume of healthy tissue  $V_{\text{Hrev}}$  and total electric current  $I$  and applied it to each electrode configuration. We examined the influence of the depth of insertion on the local electric field distribution within the target tumor tissue and its surrounding healthy tissue by visualization of the electric field and by quantification of electric distribution by calculating  $V_{\text{Trev}}$ ,  $V_{\text{Hrev}}$ ,  $V_{\text{Hirrev}}$ , and  $I$ .

TABLE II

CALCULATED VALUES OF CRITICAL VOLTAGE  $U_C$ , TOTAL ELECTRIC CURRENT  $I$ , REVERSIBLY ELECTROPERMEABILIZED TUMOR VOLUME  $V_{Trev}$ , AND REVERSIBLY AND IRREVERSIBLY ELECTROPERMEABILIZED HEALTHY TISSUE  $V_{Hrev}$  AND  $V_{Hirrev}$ , RESPECTIVELY, ARE GIVEN FOR ALL ANALYZED ELECTRODE GEOMETRIES AND POLARITIES AND FOR DEPTHS OF ELECTRODE INSERTIONS  $g = 3$  mm AND  $g = 5$  mm. ALL VOLUME VALUES ARE NORMALIZED BY THE TUMOR VOLUME  $V_T$ . DISTANCE BETWEEN OPPOSITE SETS OF ELECTRODES  $d$  AND DISTANCE BETWEEN ELECTRODES OF THE SAME ROW  $b$  (NEEDLE ELECTRODE ARRAYS) OR DISTANCE BETWEEN NEIGHBORING ELECTRODES  $b$  (HEXAGONAL NEEDLE ELECTRODE ARRAY) WERE KEPT CONSTANT AT  $b = 0.65$  mm (PARALLEL NEEDLE ELECTRODE ARRAYS),  $b = 4/\sqrt{3}$  mm (HEXAGONAL NEEDLE ELECTRODE ARRAY), AND  $d = 4$  mm, IN ALL SIMULATIONS

Electrode configuration and polarity	$g$ [mm]	$U_C$ [V]	$I$ [A]	$\frac{V_{Trev}}{V_T}$	$\frac{V_{Hrev}}{V_T}$	$\frac{V_{Hirrev}}{V_T}$
one-needle pair	5	400	0.248	1	29.96	6.14
	3	440	0.175	1	21.00	5.14
three-needle pairs	5	260	0.270	1	31.86	1.71
	3	290	0.198	1	24.86	2.35
four-needle pairs	5	240	0.294	1	43.78	2.43
	3	280	0.234	1	29.21	2.14
2x2 hexagonal array	5	290	0.301	1	38.36	3.64
	3	350	0.234	1	30.64	4.92
3x3 hexagonal array	5	280	0.463	1	42.43	9.71
	3	310	0.330	1	31.4	8.07

TABLE III

CALCULATED VALUES OF TOTAL ELECTRIC CURRENT  $I$ , REVERSIBLY ELECTROPERMEABILIZED TUMOR VOLUME  $V_{Trev}$ , AND REVERSIBLY AND IRREVERSIBLY ELECTROPERMEABILIZED HEALTHY TISSUE  $V_{Hrev}$  AND  $V_{Hirrev}$ , RESPECTIVELY, ARE GIVEN FOR ALL ANALYZED ELECTRODE GEOMETRIES AND POLARITIES AND FOR DEPTHS OF ELECTRODE INSERTIONS  $g = 3$  mm AND  $g = 5$  mm. ALL VOLUME VALUES ARE NORMALIZED BY THE TUMOR VOLUME  $V_T$ . DISTANCE BETWEEN OPPOSITE SETS OF ELECTRODES  $d$  AND DISTANCE BETWEEN ELECTRODES OF THE SAME ROW  $b$  (NEEDLE ELECTRODE ARRAYS) OR DISTANCE BETWEEN NEIGHBORING ELECTRODES  $b$  (HEXAGONAL NEEDLE ELECTRODE ARRAY) WERE KEPT CONSTANT AT  $b = 0.65$  mm (PARALLEL NEEDLE ELECTRODE ARRAYS),  $b = 4/\sqrt{3}$  mm (HEXAGONAL NEEDLE ELECTRODE ARRAY), AND  $d = 4$  mm, IN ALL SIMULATIONS. VOLTAGE WAS SET TO  $U = 290$  V IN ALL SIMULATIONS

Electrode configuration and polarity	$g$ [mm]	$U$ [V]	$I$ [A]	$\frac{V_{Trev}}{V_T}$	$\frac{V_{Hrev}}{V_T}$	$\frac{V_{Hirrev}}{V_T}$
one-needle pair	5	290	0.180	0.08	17.21	2.71
	3	290	0.115	0.03	10.42	2.00
three-needle pairs	5	290	0.301	1.00	37.21	2.79
	3	290	0.198	1.00	24.86	2.36
four-needle pairs	5	290	0.354	1.00	45.86	2.86
	3	290	0.236	1.00	30.64	2.42
2x2 hexagonal array	5	290	0.291	1.00	36.86	3.29
	3	290	0.190	0.41	22.93	2.71
3x3 hexagonal array	5	290	0.471	1.00	44.07	10.57
	3	290	0.308	0.99	29.07	7.00

Because the first part of our study showed that voltage ( $U$ ), distances between electrodes ( $b$  and  $d$ ), and depth of electrode insertion ( $g$ ) are all relevant for the distribution of electric field in the model, all four parameters were chosen for the optimization procedure. We ran the genetic algorithm for all electrode geometries and polarities in two distinct stages. In the first stage, ten runs of the algorithm were performed using a random initial population. To calculate solutions closer to the true optimum, the ten best solutions acquired from the first stage were “seeded” into the initial population of the second stage and five more solutions were calculated, all being of better fitness than the first-stage solutions. However, the difference between the best first- and second-stage solutions was less than 1% (if compared by  $V_{Hirrev}$ ); therefore, no third stage was required, and the best second stage solution was considered to be the optimum.

### III. RESULTS

The calculated critical voltage  $U_C$  needed to cover the entire tumor tissue with electric field above reversible electropermeabilization threshold  $E_{rev}$  for each electrode geometry and polarity is given in Table II. The shallower insertion of the electrodes generally increased the necessary  $U_C$ ; however, the total current  $I$  through the model decreased. Increasing the number of the electrodes had the opposite effect: Lower  $U_C$  and higher  $I$  were calculated. Both observations can be explained



Fig. 4. False color legend used in Figs. 5–7, indicating the local electric field  $E$  distribution within the tissue models (i.e., the degree of tissue electropermeabilization). The white region represents insufficiently electropermeabilized regions of tissue ( $E < E_{rev}$ ), and the patterned region represents irreversibly electropermeabilized regions of tissue ( $E > E_{irrev}$ ).

by the size of contact surface between electrodes and treated tissue—larger contact surface increases  $I$  and decreases the necessary  $U_C$ .

When we applied the same voltage (290 V) to all electrode configurations, complete electropermeabilization of the tumor was not obtained in all cases. Namely, one needle electrode pair was completely unsuccessful, whereas both hexagonal geometries did not provide adequate coverage at  $g = 3$  mm [Table III, Figs. 4, 5(a) and (b), and 6(b) and (d)]. Figs. 5 and 6 show a definite influence of electrode configuration on electric field distribution in the tumor and healthy tissue. This influence is most clearly seen by comparing electric field distributions of both hexagonal needle electrode arrays—electric field penetrates deeper for  $3 \times 3$  geometry and  $V_{Hirrev}$  is considerably larger than in  $2 \times 2$  geometry (Fig. 6). It can also be observed that deeper insertion of electrodes ( $g = 5$  mm) and insufficient voltage applied on the electrodes cause the electric field to be higher within the healthy tissue below the tumor compared to

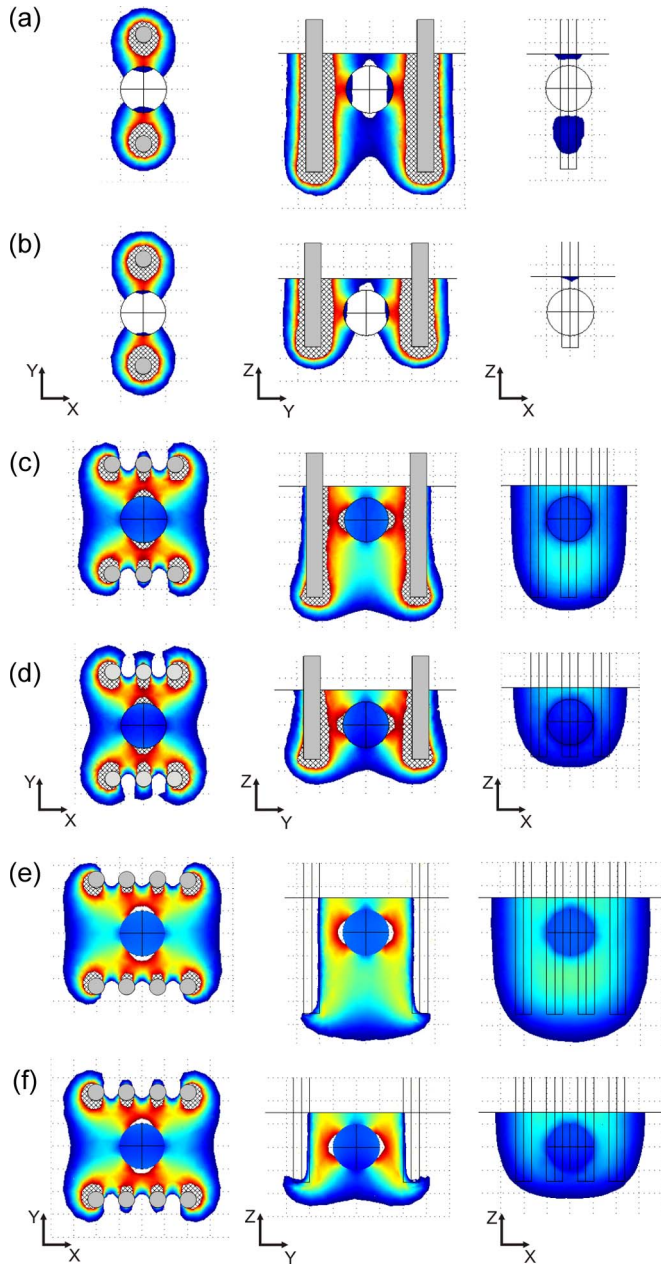


Fig. 5. Local electric field distribution for the models of (a) and (b) one needle electrode pair, (c) and (d) three needle electrode pairs, and (e) and (f) four needle electrode pairs is shown for two depths of electrodes' insertion  $g = 5$  mm [(a), (c), (e)] and  $g = 3$  mm [(b), (d), (f)]. Electric field distribution is shown in three central perpendicular planes:  $XY$ ,  $YZ$ , and  $XZ$  all passing through the center of the tumor. Distance between opposite sets of electrodes  $d$ , distance between electrodes of the same row  $b$  (needle electrode arrays) or distance between neighboring electrodes  $b$  (hexagonal needle electrode array) and voltage  $U$  are given in the caption of Table III.

the electric field inside the tumor (Fig. 5(a), (c), and (e) in  $ZX$  orientation).

To assure complete electropermeabilization of the tumor and with the least healthy tissue damage in our model, all geometrical and electrical parameters have to be accounted for. When all parameters were optimized simultaneously, the required  $U_C$  was significantly lower (Table IV) than when determining the  $U_C$  for only two depths of needle insertion (Table II). At the same time,  $I$ ,  $V_{Hrev}$ , and  $V_{Hirrev}$  were also

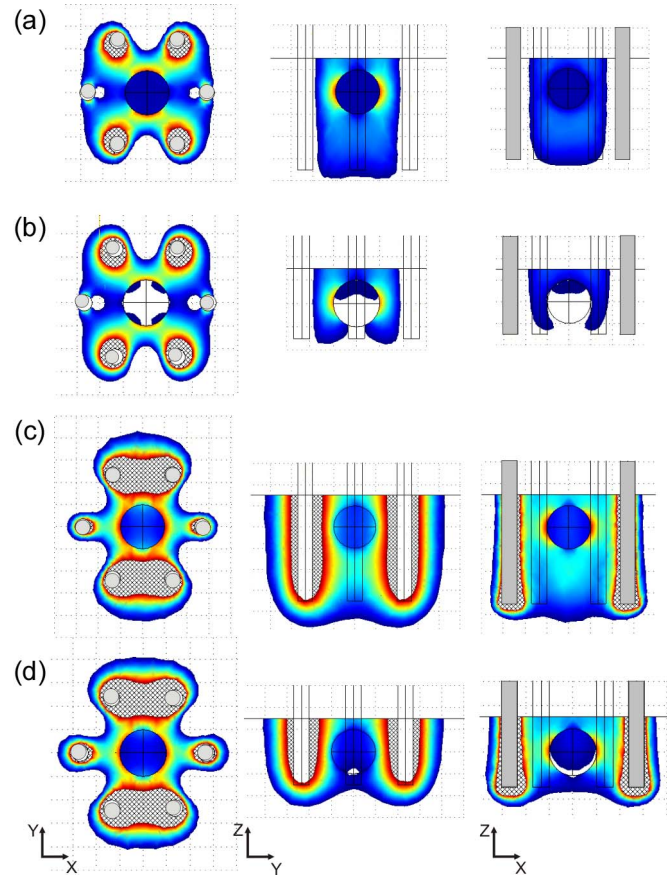


Fig. 6. Local electric field distribution for the models of (a) and (b)  $2 \times 2$  hexagonal needle electrode array and (c) and (d)  $3 \times 3$  hexagonal needle electrode array is shown for two depths of electrodes' insertion  $g = 5$  mm [(a), (c)] and  $g = 3$  mm [(b), (d)]. Electric field distribution is shown in three central perpendicular planes:  $XY$ ,  $YZ$ , and  $XZ$  all passing through the center of the tumor. Distance between opposite sets of electrodes  $d$ , distance between electrodes of the same row  $b$  (needle electrode arrays) or distance between neighboring electrodes  $b$  (hexagonal needle electrode array) and voltage  $U$  are given in the caption of Table III.

decreased, thus minimizing healthy tissue damage and required electric energy. Interestingly, the optimum depth of insertion depended very much on the electrode geometry, i.e., at similar applied voltages, the  $2 \times 2$  hexagonal needle electrode array has to be inserted deeper than the  $3 \times 3$  needle electrode array to achieve similar coverage of the target tumor tissue. The results of optimization using our algorithm are shown in Table IV and Fig. 7.

#### IV. DISCUSSION AND CONCLUSION

The aim of our study was to investigate and optimize the local electric field within a simple 3-D model of a subcutaneous tumor. We report the results of optimization of the geometrical and electrical parameters (voltage, distances between electrodes, depth of electrode insertion:  $U$ ,  $b$ ,  $d$ , and  $g$ ; Figs. 1 and 3) of various needle electrode geometries used in research and clinical ECT for a 3-D numerical model of a subcutaneous tumor (Fig. 2). We show by using our optimization algorithm, how the local electric field distribution depends on the number, arrangement, depth of electrodes' insertion, and the amplitude

TABLE IV

OPTIMIZED VALUES OF DISTANCE BETWEEN ELECTRODES OF THE SAME ROW  $b$  (NEEDLE ELECTRODE ARRAYS), DISTANCE BETWEEN NEIGHBORING ELECTRODES  $b$  (HEXAGONAL NEEDLE ELECTRODE ARRAY), DISTANCE BETWEEN OPPOSITE SETS OF ELECTRODES  $d$ , DEPTH OF ELECTRODES' INSERTION  $g$ , AND CRITICAL VOLTAGE  $U_C$  FOR ALL ANALYZED ELECTRODE GEOMETRIES AND POLARITIES ARE GIVEN. CALCULATED VALUES OF TOTAL ELECTRIC CURRENT  $I$ , REVERSIBLY ELECTROPERMEABILIZED TUMOR VOLUME  $V_{Trev}$ , REVERSIBLY AND IRREVERSIBLY ELECTROPERMEABILIZED HEALTHY TISSUE  $V_{Hrev}$  AND  $V_{Hirrev}$ , RESPECTIVELY, ARE GIVEN FOR ALL OPTIMUM SOLUTIONS. ALL VOLUME VALUES ARE NORMALIZED BY THE TUMOR VOLUME  $V_T$

Electrode configuration and polarity	$b$ [mm]	$d$ [mm]	$g$ [mm]	$U_C$ [V]	$I$ [A]	$V_{Trev}/V_T$	$V_{Hrev}/V_T$	$V_{Hirrev}/V_T$
three-needle pairs	0.70	4.04	3.15	272	0.20	1	23.64	1.86
four-needle pairs	0.67	4.10	3.20	265	0.25	1	28.29	1.65
2x2 hexagonal array	1.71	3.47	3.57	256	0.24	1	21.86	2.34
3x3 hexagonal array	1.71	3.47	2.90	246	0.32	1	21.64	5.14

of electric pulses (Figs. 5–7, Tables II–IV). The complete coverage of the target tumor tissue with the local electric field magnitude required for successful ECT ( $E_{rev} < E < E_{irrev}$ ) was achieved, whereas the volumes of healthy tissue exposed to the magnitude of the local electric field above reversible and irreversible thresholds were minimized (thus minimizing healthy tissue damage) for all analyzed electrode geometries.

Our study was built on previous research works done by our group and others, in which the usefulness of numerical modeling in predicting electropermeabilization outcomes was demonstrated. Already, the early numerical plate and needle electrode models in combination with *in vivo* experiments showed great promise in analysis of tissue electropermeabilization *in vivo* [18], [25]. However, only after the experimental validation of a numerical model was performed by comparing the numerical calculations to histological examinations of electropermeabilized tissue did numerical modeling gain ground in ECT research [11]. Different geometries of needle electrodes have been since then compared by [14], [26], and [27]; however, none of these included optimization and only Sel *et al.* [28] used a 3-D model. In our study, three needle electrode pairs, four needle electrode pairs, and  $2 \times 2$  hexagonal needle electrode array all gave similar results, whereas the  $3 \times 3$  hexagonal needle electrode array was significantly worse than the others. We examined the adequacy of needle electrode geometries by calculating values of total electric current through the model and volumes of reversibly and irreversibly electropermeabilized (damaged) healthy tissue. By analyzing all three measures, we can conclude that three needle electrode pairs gave the best results—they required the lowest total electric current, which caused a small volume of healthy tissue to be reversibly and even less to be irreversibly electropermeabilized (Fig. 7(a), Table IV). Four needle electrode pairs caused the

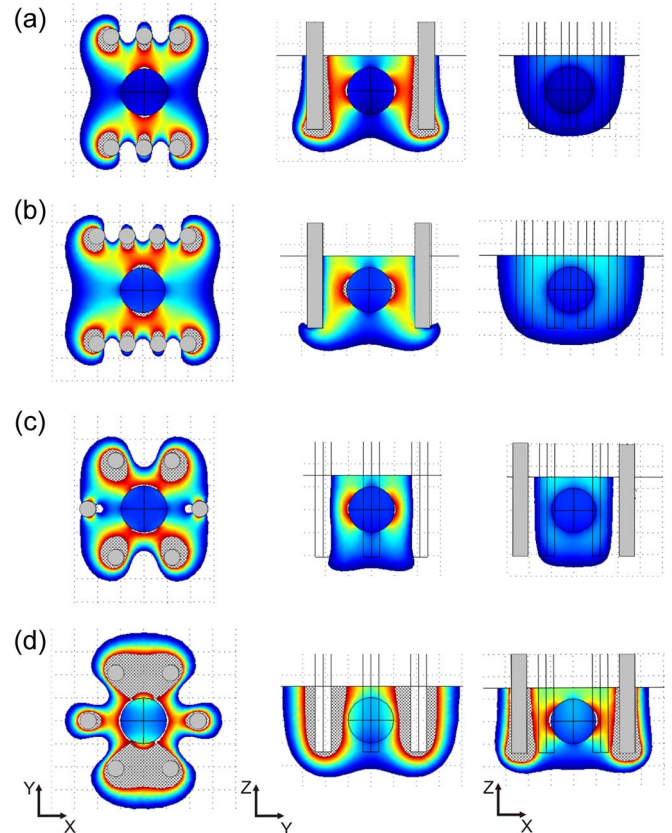


Fig. 7. Local electric field distribution for the optimized models of (a) three needle electrode pairs, (b) four needle electrode pairs, (c)  $2 \times 2$  hexagonal needle electrode array, and (d)  $3 \times 3$  hexagonal needle electrode array is shown. The electric field distribution is shown in three central perpendicular planes:  $XY$ ,  $YZ$ , and  $XZ$  all passing through the center of the tumor. Corresponding optimized parameters which are distance between electrodes of the same row  $b$  (needle electrode arrays), distance between neighboring electrodes  $b$  (hexagonal needle electrode array), distance between opposite sets of electrodes  $d$ , depth of electrodes' insertion  $g$ , and critical voltage  $U_C$  are given in Table IV.

least healthy tissue damage; however, they required more current and more healthy tissue to be reversibly electropermeabilized (Fig. 7(b), Table IV), confirming previous results of our group—more electrodes mean a more invasive procedure, higher needed current, and lower needed voltage to obtain the same target tissue coverage [11], [26]. The  $2 \times 2$  hexagonal needle electrode array caused the least volume of healthy tissue to be reversibly electropermeabilized and more to be irreversibly electropermeabilized (Fig. 7(c), Table IV). The  $3 \times 3$  hexagonal needle electrode array optimization lead to the highest values of total electric current and the largest area of irreversibly permeabilized healthy tissue (Fig. 7(d), Table IV). The preference for three needle electrode pairs is also in agreement with our previous 2-D study [27].

The only other ECT optimization study was performed by Sel *et al.* who optimized the distance and voltage between electrodes for a realistic brain tumor using four pairs of needle electrodes as a proof of principle [28]. In our study, we used a simpler tumor model; however, we took the optimization one step further by optimizing for four different electrode geometries and polarities and for four different parameters, one of them being the depth of needle insertion, which turned

out to be significant. We demonstrated that inserting needle electrodes deeper than necessary, using inadequate electrode geometries, polarities, and arrangement with respect to the target tumor tissue, and applying insufficient voltage can result in unsuccessful electropermeabilization ( $E < E_{rev}$ ) of the tumor. Moreover, the electric field within the healthy tissue below the tumor can be higher compared to the electric field inside the tumor [Figs. 5(a) and 6(d)]. This effect can be even more pronounced if the tumor is much more conductive than the surrounding tissue, because the electric field is then lower in the tumor and higher in the surrounding tissue [27]. The importance of insertion depth can also be seen if we compare the optimum depth for hexagonal needle electrode arrays—deeper insertion is required for the  $2 \times 2$  needle electrode array, although all other geometrical parameters are the same for both configurations.

Even though our algorithm gives good results, significant challenges remain before it can be used for the optimization of *in vivo* ECT of large tumors. Our study does not analyze the possibility of changing electric field orientation in consecutive pulses, which can lead to less tissue damage, because such protocols can require lower voltage and total current [14]. Unfortunately, increasing the number of pulses can increase the unpleasantness of the treatment [29]. We also did not take into account the dynamic changes in tissue conductivities due to the tissue electropermeabilization [19], [28], [30] because this would significantly increase the computation time and would not considerably contribute to the results. Instead, we incorporated the change in conductivity into our model by choosing conductivity values at the end of the electropermeabilization process. Stratum corneum was not added to the model, as needle electrodes penetrate the skin and thus bypass its high resistivity [13]; however, if plate electrodes were to be used, we would most probably have to take into account also the stratum corneum and the skin conductivity changes due to electropermeabilization.

We chose the genetic algorithm as our optimization method, as it is relatively easy to develop and, unlike classical optimization methods, it does not require the fitness function to be differentiable. Linear and nonlinear constraints, such as the realistic technical limitations of high-voltage electric pulse generator (maximum output voltage and current), can be easily implemented into the algorithm, and it also allows optimization of a large number of continuous, discrete, and categorical parameters, e.g., type of electrodes. The drawbacks of the method are that it gives only an approximate solution to the optimization problem and requires a relatively long computation time. However, because the solutions of the algorithm are very close to the true optimum and computation times can be shortened by using a more powerful computer, we do not consider these to be significant drawbacks and believe that the suggested approach is well suited to the problem being addressed.

Numerical modeling and optimization can be efficiently combined to control the extent of tissue electropermeabilization in ECT and to produce the optimum electrode configuration for different types of tumors taking into account their electric properties. Our algorithm is a step forward to an effective treatment planning, not only in clinical ECT, but also in other

electroporation-based treatments, such as gene electrotransfer [19], transdermal drug delivery [20], and irreversible tumor ablation [21].

## REFERENCES

- [1] M. Marty, G. Sersa, J. R. Garbay, J. Gehl, C. G. Collins, M. Snoj, V. Billard, P. F. Geertsens, J. O. Larkin, D. Miklavcic, I. Pavlovic, S. M. Paulin-Kosir, M. Cemazar, N. Morsli, Z. Rudolf, C. Robert, G. C. O'Sullivan, and L. M. Mir, "Electrochemotherapy—An easy, highly effective and safe treatment of cutaneous and subcutaneous metastases: Results of ESOPE (European Standard Operating Procedures of Electrochemotherapy) study," *Eur. J. Cancer, Suppl.*, vol. 4, no. 11, pp. 3–13, Nov. 2006.
- [2] G. Sersa, "The state-of-the-art of electrochemotherapy before the ESOPE study; advantages and clinical uses," *Eur. J. Cancer, Suppl.*, vol. 4, no. 11, pp. 52–59, Nov. 2006.
- [3] R. Heller, R. Gilbert, and M. J. Jaroszeski, "Clinical applications of electrochemotherapy," *Adv. Drug Deliv. Rev.*, vol. 35, no. 1, pp. 119–129, Jan. 1999.
- [4] A. Gothelf, L. M. Mir, and J. Gehl, "Electrochemotherapy: Results of cancer treatment using enhanced delivery of bleomycin by electroporation," *Cancer Treat. Rev.*, vol. 29, no. 5, pp. 371–387, Oct. 2003.
- [5] B. M. Tjink, R. De Bree, G. Van Dongen, and C. R. Leemans, "How we do it: Chemo-electroporation in the head and neck for otherwise untreatable patients," *Clin. Otolaryngol.*, vol. 31, no. 5, pp. 447–451, Oct. 2006.
- [6] L. M. Mir, J. Gehl, G. Sersa, C. G. Collins, J. R. Garbay, V. Billard, P. F. Geertsens, Z. Rudolf, G. C. O'Sullivan, and M. Marty, "Standard operating procedures of the electrochemotherapy: Instructions for the use of bleomycin or cisplatin administered either systemically or locally and electric pulses delivered by the Cliniporator by means of invasive or non-invasive electrodes," *Eur. J. Cancer, Suppl.*, vol. 4, no. 11, pp. 14–25, Nov. 2006.
- [7] M. Snoj, Z. Rudolf, M. Cemazar, B. Jancar, and G. Sersa, "Successful sphincter-saving treatment of anorectal malignant melanoma with electrochemotherapy, local excision and adjuvant brachytherapy," *Anti-Cancer Drugs*, vol. 16, no. 3, pp. 345–348, Mar. 2005.
- [8] G. Sersa, M. Cemazar, D. Miklavcic, and Z. Rudolf, "Electrochemotherapy of tumours," *Radiol. Oncol.*, vol. 40, no. 3, pp. 163–174, 2006.
- [9] C. Domenge, S. Orłowski, B. Luboinski, T. De Baere, G. Schwaab, J. Belehradek, and L. M. Mir, "Antitumor electrochemotherapy: New advances in the clinical protocol," *Cancer*, vol. 77, no. 5, pp. 956–963, Mar. 1996.
- [10] D. Miklavcic, K. Beravs, D. Semrov, M. Cemazar, F. Demsar, and G. Sersa, "The importance of electric field distribution for effective *in vivo* electroporation of tissues," *Biophys. J.*, vol. 74, no. 5, pp. 2152–2158, May 1998.
- [11] D. Miklavcic, D. Semrov, H. Mekid, and L. M. Mir, "A validated model of *in vivo* electric field distribution in tissues for electrochemotherapy and for DNA electrotransfer for gene therapy," *Biochim. Biophys. Acta*, vol. 1523, no. 1, pp. 73–83, Sep. 2000.
- [12] M. Puc, S. Corovic, K. Flisar, M. Petkovsek, J. Nastran, and D. Miklavcic, "Techniques of signal generation required for electropermeabilization. Survey of electropermeabilization devices," *Bioelectrochemistry*, vol. 64, no. 2, pp. 113–124, Sep. 2004.
- [13] D. Miklavcic, S. Corovic, G. Pucihar, and N. Pavsclj, "Importance of tumour coverage by sufficiently high local electric field for effective electrochemotherapy," *Eur. J. Cancer, Suppl.*, vol. 4, no. 11, pp. 45–51, Nov. 2006.
- [14] R. A. Gilbert, M. J. Jaroszeski, and R. Heller, "Novel electrode designs for electrochemotherapy," *Biochim. Biophys. Acta*, vol. 1334, no. 1, pp. 9–14, Feb. 1997.
- [15] J. F. Edd, L. Horowitz, R. V. Davalos, L. M. Mir, and B. Rubinsky, "In vivo results of a new focal tissue ablation technique: Irreversible electroporation," *IEEE Trans. Biomed. Eng.*, vol. 53, no. 7, pp. 1409–1415, Jul. 2006.
- [16] N. Pavsclj, Z. Bregar, D. Cukjati, D. Batiuskaite, L. Mir, and D. Miklavcic, "The course of tissue permeabilization studied on a mathematical model of a subcutaneous tumor in small animals," *IEEE Trans. Biomed. Eng.*, vol. 52, no. 8, pp. 1373–1381, Aug. 2005.
- [17] D. Miklavcic, N. Pavsclj, and F. X. Hart, "Electric properties of tissues," in *Wiley Encyclopedia of Biomedical Engineering*. New York: Wiley, 2006.
- [18] J. Gehl, T. H. Sorensen, K. Nielsen, P. Raskmark, S. L. Nielsen, T. Skovsgaard, and L. M. Mir, "In vivo electroporation of skeletal muscle:

- Threshold, efficacy and relation to electric field distribution," *Biochim. Biophys. Acta*, vol. 1428, no. 2, pp. 233–240, Aug. 1999.
- [19] D. Cukjati, D. Batiuskaite, F. Andre, D. Miklavcic, and L. M. Mir, "Real time electroporation control for accurate and safe in vivo non-viral gene therapy," *Bioelectrochemistry*, vol. 70, no. 2, pp. 501–507, May 2007.
- [20] U. F. Pliquet, R. Vanbever, V. Preat, and J. C. Weaver, "Local transport regions (LTRs) in human stratum corneum due to long and short "high voltage" pulses," *Bioelectrochem. Bioenerg.*, vol. 47, no. 1, pp. 151–161, Nov. 1998.
- [21] B. Al-Sakere, C. Bernat, E. Connault, P. Opolon, B. Rubinsky, R. Davalos, and L. M. Mir, "Tumor ablation with irreversible electroporation," *PLoS ONE*, vol. 2, no. 11, p. e1135, 2007.
- [22] D. Semrov and D. Miklavcic, "Calculation of the electrical parameters in electrochemotherapy of solid tumours in mice," *Comput. Biol. Med.*, vol. 28, no. 4, pp. 439–448, Jul. 1998.
- [23] J. H. Holland, *Adaptation in Natural and Artificial Systems: An Introductory Analysis With Applications to Biology, Control, and Artificial Intelligence*. Cambridge, MA: MIT Press, 1992.
- [24] J. Gehl and P. F. Geertsen, "Palliation of haemorrhaging and ulcerated cutaneous tumours using electrochemotherapy," *Eur. J. Cancer, Suppl.*, vol. 4, no. 11, pp. 35–37, Nov. 2006.
- [25] G. Sersa, M. Cemazar, D. Semrov, and D. Miklavcic, "Changing electrode orientation improves the efficacy of electrochemotherapy of solid tumors in mice," *Bioelectrochem. Bioenerg.*, vol. 39, no. 1, pp. 61–66, Feb. 1996.
- [26] D. Sel, S. Mazeres, J. Teissie, and D. Miklavcic, "Finite-element modeling of needle electrodes in tissue from the perspective of frequent model computation," *IEEE Trans. Biomed. Eng.*, vol. 50, no. 11, pp. 1221–1232, Nov. 2003.
- [27] S. Corovic, M. Pavlin, and D. Miklavcic, "Analytical and numerical quantification and comparison of the local electric field in the tissue for different electrode configurations," *Biomed. Eng. Online*, vol. 6, no. 1, p. 37, 2007.
- [28] D. Sel, A. M. Lebar, and D. Miklavcic, "Feasibility of employing model-based optimization of pulse amplitude and electrode distance for effective tumor electroporation," *IEEE Trans. Biomed. Eng.*, vol. 54, no. 5, pp. 773–781, May 2007.
- [29] A. Zupanic, S. Ribaric, and D. Miklavcic, "Increasing the repetition frequency of electric pulse delivery reduces unpleasant sensations that occur in electrochemotherapy," *Neoplasma*, vol. 54, no. 3, pp. 246–250, 2007.
- [30] R. V. Davalos, B. Rubinsky, and D. M. Otten, "A feasibility study for electrical impedance tomography as a means to monitor tissue electroporation for molecular medicine," *IEEE Trans. Biomed. Eng.*, vol. 49, no. 4, pp. 400–403, Apr. 2002.



**Anze Zupanic** was born in 1981. He received the B.Sc. degree in electrical engineering from the University of Ljubljana, Ljubljana, Slovenia, where he is currently working toward the Ph.D. degree in electrical engineering in the Faculty of Electrical Engineering.

He is a Young Researcher with the Faculty of Electrical Engineering, University of Ljubljana. His main research interests are multiphysics numerical modeling and optimization of electroporation-based treatments.



**Damijan Miklavcic** was born in Ljubljana, Slovenia, in 1963. He received the Ph.D. degree in electrical engineering from the University of Ljubljana, Ljubljana.

He is a Professor with the Faculty of Electrical Engineering, University of Ljubljana, and the Head of the Laboratory of Biocybernetics. He is active in the field of biomedical engineering. His interest in the last years focuses on electroporation-assisted drug and gene delivery, including cancer treatment by means of electrochemotherapy, tissue oxygenation, modeling of biological processes, and hardware development.



**Selma Corovic** was born in 1976. She received the B.Sc. and M.Sc. degrees in electrical engineering from the University of Ljubljana, Ljubljana, Slovenia. She is currently working toward the Ph.D. degree at the Faculty of Electrical Engineering, University of Ljubljana and at the Paris University-Sud XI, Châtenay-Malabry 92 296, France.

She is an Assistant Researcher with the Faculty of Electrical Engineering, University of Ljubljana. Her main research interests are multiphysics numerical modeling and *in vivo* studies of electroporation

process in biological tissues and web-based e-learning application development for electroporation-based treatments.